NEW HIGH ACCURACY DETERMINATION OF RANGE AND RANGE RATE OF SATELLITES FROM EISCAT RADAR DATA TAKEN DURING 2010 SSA CO-VI CAMPAIGN

J. Markkanen[(1)]**, T. Nygrén**[(2)]**, and M. Markkanen**[(3)]

[(1)]*EISCAT, Tähteläntie 54B, 99600 Sodankylä, Finland, Email: Jussi.Markkanen@sgo.fi*
[(2)]*Department of Physics,University of Oulu, P.O. Box 3000, 90014, Finland, Email: Tuomo.Nygren@oulu.fi*
[(3)]*Eigenor Corporation, Lompolontie 1, 99600 Sodankylä, Finland, Email: Markku.Markkanen@eigenor.com*

ABSTRACT

We have developed further the methods used in EISCAT for analysing radar measurements of space debris, and have re-analysed part of the satellite data taken in 2010 during SSA CO-VI campaign. The updated analysis makes Bayesian estimates of range and range rate, and includes proper error analysis which was largely missing in the earlier work. The new analysis achieves centimetres per second statistical accuracy in range rate by determining the maximum of the the continuous-ω periodogram, and achieves a few tens of centimetres statistical accuracy in range by utilising the detailed shape of the receiver impulse response. Systematic errors remain to be fixed, but even as it is, the new analysis improves the accuracy of the range and range rate estimates between one and two orders of magnitude.

Key words: space debris; Bayesian analysis; sub-sample resolution.

1. THE PROBLEM IN EISCAT STANDARD SPACE DEBRIS DATA PROCESSING

In space debris work done in EISCAT under several ESA contracts in 2000–2006, target's range and range rate were estimated essentially by finding the position of the maximum of the two-dimensional radar ambiguity function, which we have been calling the match function $MF(R, \omega)$ [4, 5]. In that work, the MF maximum position was determined by searching over a discrete grid of range and frequency values. This approach is fast, and sufficient for typical space debris targets, but the quantisation in R and ω seriously limits the attainable accuracy when signal to noise ratio is very high.

In range direction the discretization is due to signal sampling (now with 1 μs sampling interval). In frequency direction, the quantisation results from the discrete Fourier transform, with modest zero-padding, used in evaluating the MF. The standard analysis was applied to the satellite measurements taken in December 2010 during the SSA Preparatory Phase CO-VI campaign. The standard analysis does not give proper error estimates, and what was quoted for the analysed data was residual r.m.s variations of range and velocity fits during a beam pass. Even in cases with signal to noise ratio of several thousands, the quoted accuracy of range was only of the order of one half of the sampling interval, some 50 metres, and the quoted Doppler-accuracy was of the order of a one metre per second. To our understanding, when the EISCAT 2011 results were evaluated for orbit determination purposes [3], only the range results were used, the Doppler-data having been considered too inaccurate.

2. THE UPDATED ANALYSIS METHOD

2.1. Bayesian method for determining range and range rate and their errors

In order to achieve both optimal accuracy and well-defined error estimates, we use Bayesian statistical inference in a two-step procedure. We first determine range and range rate from individual transmitted-received pulses together with their statistical errors. Then we use the results from the several hundred pulses of a typical beam-pass event to produce the final range and range rate values and their errors.

The starting point is a parametrized signal model, and the aim is to make a statistically correct fit of the model to the measured data. For a single pulse, about two milliseconds long in this case, we can assume constant target velocity. By referring the per-pulse velocity to the centre point of the pulse, this also takes correctly into account a linear variation of range rate during the pulse. We model the received signal by a replicate of the transmission which is both delayed in time and Doppler-shifted in frequency. In particular, we consider reflection from a point target so that we do not take into account the actual target size. In our derivation below, we ignore various back-and-forth frequency translations in the radar system and write the formulas for the base-band signals. During

the 2010 campaign, the EISCAT receiver sampled continuously with 1 μs sampling interval, providing samples at this rate both from the transmitted pulse and the received echo. The number of samples per each 1920 μs pulse was thus (about) 1920. The pulse repetition frequency of 20 ms was used. The baud length of the phase code was 60 μs.

The samples z_m of the complex-valued base-band radar echo during the reception of a single echo pulse are modelled by

$$z_m = A\epsilon(t_m - 2R/c)\exp(i\omega t_m) + \gamma_m. \quad (1)$$

Here A is a complex constant, ϵ is a filtered real-valued phase modulation pattern, t_m is the sampling time, R is the range, ω is the angular Doppler-frequency and γ_m is the noise term. The amplitude A contains both the phase variation along the signal path and all factors affecting the signal amplitude, including a possible amplitude droop. The argument of the phase modulation ϵ contains the time delay from transmitter to target and back, and the modulation has unit magnitude except at the slopes near the phase flips. These slopes are due to filtering in the receiver. The angular frequency is given by $\omega = -2v_r\,\omega_{\mathrm{r}}/c$, where v_r is the radial target velocity and ω_r is the radar angular frequency. The noise term γ_m is taken to obey Gaussian noise with a variance $\sigma^2 = |A|^2/\mathrm{SNR}$, where SNR is the signal-to-noise ratio of the received signal. The value of SNR is estimated separately using samples from times with no echo signal.

The number of samples from a single pulse is denoted by M. We collect the various quantities in Eq. (1) into M-point column vectors

$$\mathbf{z} = (z_0, \ldots, z_{\mathrm{M}-1})^{\mathrm{T}}$$
$$\boldsymbol{\epsilon}(R) = [\epsilon(t_0 - 2R/c), \ldots, \epsilon(t_{\mathrm{M}-1} - 2R/c)]^{\mathrm{T}}$$
$$\boldsymbol{\xi}(\omega) = [\exp(i\omega t_0), \ldots, \exp(i\omega t_{\mathrm{M}-1})]^{\mathrm{T}}$$

and denote the standard inner product of complex vectors $\mathbf{x}$ and $\mathbf{y}$ as

$$\mathbf{x} \cdot \mathbf{y} = \sum_{m=0}^{M-1} x_m \overline{y}_m.$$

For brevity, we also denote the point-wise product of $\epsilon(R)$ and $\boldsymbol{\xi}(\omega)$ by

$$\boldsymbol{\Xi}(R, \omega) = \boldsymbol{\epsilon}(R) \odot \boldsymbol{\xi}(\omega) = (\epsilon_0 \xi_0, \ldots, \epsilon_{\mathrm{M}-1} \xi_{\mathrm{M}-1})^{\mathrm{T}}.$$

When the samples at the phase flips are skipped, the norm of $\boldsymbol{\Xi}$ is independent of R and ω, i.e.

$$\|\boldsymbol{\Xi}\|^2 = \boldsymbol{\Xi} \cdot \boldsymbol{\Xi} \approx M. \quad (2)$$

The Bayesian solution for the model parameters A, R and ω proceeds as follows. With non-informative priors, the posterior probability density for parameters, given the measurement, is

$$p(A, R, \omega | \mathbf{z}) \propto \exp\left\{ -\frac{\|\mathbf{z} - A\,\boldsymbol{\epsilon}(R) \odot \boldsymbol{\xi}(\omega)\|^2}{\sigma^2} \right\}$$
$$= \exp\left\{ -\frac{\|\mathbf{z} - A\boldsymbol{\Xi}(R,\omega)\|^2}{\sigma^2} \right\}. \quad (3)$$
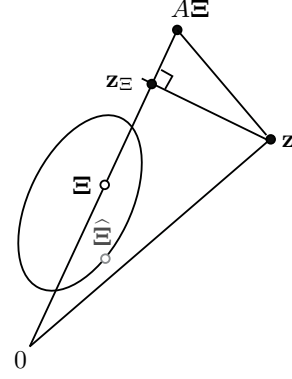

Figure 1. Geometric interpretation of the range and frequency estimation problem in terms of vectors in the linear space $\mathbb{C}^M$. Measured echo+noise vector $\mathbf{z}$ and a set of basic echo model vectors $\{\boldsymbol{\Xi}(R,\omega)\}$, which is extended linearly to the full set of model vectors $\{A\boldsymbol{\Xi}\}$. $\mathbf{z}_{\boldsymbol{\Xi}}$ is the orthogonal projection of $\mathbf{z}$ onto $\boldsymbol{\Xi}$. The best estimate $\widehat{\boldsymbol{\Xi}}$ is the element of $\{\boldsymbol{\Xi}\}$ that is as parallel to $\mathbf{z}$ as possible (there can be elements in the basic set which are nearer to $\mathbf{z}$ than $\widehat{\boldsymbol{\Xi}}$). At $\widehat{\boldsymbol{\Xi}}$, $\mathbf{z}_{\boldsymbol{\Xi}}$ attains its maximum length.

With reference to Fig. 1 and the Pythagorean theorem, the norm squared in Eq. (3) is expanded as

$$\|\mathbf{z} - A\boldsymbol{\Xi}\|^2 = \|A\boldsymbol{\Xi} - \mathbf{z}_{\boldsymbol{\Xi}}\|^2 + \|\mathbf{z} - \mathbf{z}_{\boldsymbol{\Xi}}\|^2. \quad (4)$$

where $\mathbf{z}_{\boldsymbol{\Xi}}$ is the orthogonal projection of $\mathbf{z}$ onto $\boldsymbol{\Xi}$,

$$\mathbf{z}_{\boldsymbol{\Xi}} = \frac{\mathbf{z} \cdot \boldsymbol{\Xi}}{\|\boldsymbol{\Xi}\|^2}\boldsymbol{\Xi} = \frac{\mathbf{z} \cdot \boldsymbol{\Xi}}{M}\boldsymbol{\Xi}. \quad (5)$$

Using Eq. (5) and Eq. (2), the first term on the right-hand side of Eq. (4) becomes

$$\|A\boldsymbol{\Xi} - \mathbf{z}_{\boldsymbol{\Xi}}\|^2 = M\left| A - \frac{\mathbf{z} \cdot \boldsymbol{\Xi}}{M} \right|^2. \quad (6)$$

Using the Pythagorean theorem for a second time, the second term on the right-hand side of Eq. (4) becomes

$$\|\mathbf{z} - \mathbf{z}_{\boldsymbol{\Xi}}\|^2 = \|\mathbf{z}\|^2 - \|\mathbf{z}_{\boldsymbol{\Xi}}\|^2$$
$$= \|\mathbf{z}\|^2 - \frac{|\mathbf{z} \cdot \boldsymbol{\Xi}|^2}{M}. \quad (7)$$

Collecting these results, the posteriori density is

$$p(A, R, \omega | \mathbf{z}) = C_z \exp\left\{ -\frac{M}{\sigma^2}\left| A - \frac{\mathbf{z} \cdot \boldsymbol{\Xi}(R, \omega)}{M} \right|^2 \right\}$$
$$\times \exp\left\{ \frac{|\mathbf{z} \cdot \boldsymbol{\Xi}(R, \omega)|^2}{M\sigma^2} \right\}. \quad (8)$$

where C_z is a probability-normalising constant.

With the measurement $\mathbf{z}$ fixed, the parameter values that maximise the posterior probability—the MAP, maximum a posteriori, estimate—are found from Eq. (8)

by simultaneously maximising $|\mathbf{z} \cdot \boldsymbol{\Xi}|^2$, and minimising $|A - \mathbf{z} \cdot \boldsymbol{\Xi}/M|^2$ to its absolute minimum, zero. The MAP estimate is

$$(\widehat{R}, \widehat{\omega}) = \arg\max_{R,\omega} \frac{|\mathbf{z} \cdot \boldsymbol{\Xi}(R,\omega)|^2}{\|\boldsymbol{\Xi}(R,\omega)\|^2} \qquad (9)$$

and

$$\widehat{A} = \frac{\mathbf{z} \cdot \boldsymbol{\Xi}(\widehat{R}, \widehat{\omega})}{\|\boldsymbol{\Xi}(\widehat{R}, \widehat{\omega})\|^2} \, . \qquad (10)$$

For error estimates of the parameters, we use the posterior variances computed from Eq. (8). For error estimates of $\widehat{R}$ and $\widehat{\omega}$, we marginalise Eq. (8) by integrating over A for all values of $A = A_r + iA_i$; that is, both over the real part and imaginary parts from $-\infty$ to $+\infty$. The factor in Eq. (8) that depends on A splits into two exponentials

$$\exp\left\{ -\frac{|\boldsymbol{\Xi}^2|}{\sigma^2} \left| A - \frac{\mathbf{z} \cdot \boldsymbol{\Xi}}{\|\boldsymbol{\Xi}\|^2} \right|^2 \right\} =$$
$$\exp\left\{ -\frac{\|\boldsymbol{\Xi}\|^2 (A_r - a_r)^2}{\sigma^2} \right\} \times \exp\left\{ -\frac{\|\boldsymbol{\Xi}\|^2 (A_i - a_i)^2}{\sigma^2} \right\}$$
$$(11)$$

where a_r and a_i are the real and imaginary parts of $\mathbf{z} \cdot \boldsymbol{\Xi}/\|\boldsymbol{\Xi}\|^2$. The integral

$$\int_{-\infty}^{\infty} dA_k \exp\left[-\frac{\|\boldsymbol{\Xi}\|^2 (A_k - a_k)^2}{\sigma^2} \right] \qquad (12)$$

is readily evaluated and does not depend on a_k. Neither does it depend on R or ω since, with the usually good approximation in Eq. (2), $\|\boldsymbol{\Xi}\|^2$ is constant. Then the over signal amplitude marginalised posteriori density takes the particularly simple form

$$p(R, \omega | \mathbf{z}) = C_z \exp\left[\frac{|\mathbf{z} \cdot \boldsymbol{\Xi}(R,\omega)|^2}{M\sigma^2} \right] \, . \qquad (13)$$

To the degree that the model functions $\boldsymbol{\Xi}(R, \omega)$ are known and correct, equations Eq. (9) and (13) provide a complete, well-defined Bayesian solution for the range and range rate estimation problem. This two-parameter model is approximate, and here it is defined for a single pulse only. In the case of weak space debris targets, coherent integration would be needed. Then the data vector would contain multiple pulses and the model would contain a larger number of parameters.

The problem is how to calculate $\widehat{R}$ and $\widehat{\omega}$ in Eq. (9) and their error estimates at a high numerical accuracy. Our current way of making use of Eq. (9) and (13) proceeds in several steps. We first apply these equations to a single transmission-reception cycle at a time. In typical satellite beam pass events, lasting a few seconds, we get hundreds of such single-pulse estimates. Then these are used to further improve the accuracy. Before describing the single-pulse processing in more detail, we summarise the fairly standard way of how these single-pulse values are used to produce the final analysis results.

3. COMBINING SINGLE-PULSE ANALYSIS RESULTS

The single-pulse range and range rate values and their errors are used as input in a separate Bayesian estimation problem. This step is equivalent to a weighted least squares fit of a (vector-valued) model function $[R(T), v(T)]$ to the beam pass data. As the model function for range measurements $(T_n, \widehat{R}_n)$ during a single beam pass, we use a third-order polynomial of (UTC-) time T,

$$\widehat{R}_n = a\,T_n^3 + b\,T_n^2 + c\,T_n + d \,, n = 1 \ldots N_r \, . \qquad (14)$$

The time derivative of Eq. (14) is used as a model function for the single-pulse range rate measurements (T_k, v_k)

$$\widehat{v}_k = 3a\,T_k^2 + 2b\,T_k + c \,, k = 1 \ldots N_v \, . \qquad (15)$$

The inverses of the variances $\sigma^2(\widehat{R}_n)$ and $\sigma^2(\widehat{v}_k)$ of the single-pulse range and range range estimates $\widehat{R}_n$ and $\widehat{v}_k$ are used as the weights of the data points. Eq. (14) and (15) provide a linear system of $N_r + N_v$ equations for the four unknown model coefficients a, b, c and d, which we solve using standard matrix formalism, taking into account the weights. Details of the procedure are given in [6]. With the presumption that the weights represent independent Gaussian errors, the solution provides Bayesian estimates of the four model coefficients and their errors, and allows one to estimate the range and range rate for any desired instant of time, with error estimates. As the final analysis results we tabulate, for each beam pass event, a single range and range rate value and their 1-sigma errors, and the associated UTC instant of time.

4. SINGLE-PULSE ANALYSIS

4.1. Grid search to get initial estimates

The first step is to find good initial estimates for the range and the Doppler frequency from Eq. (9). We do this simply by making an exhaustive grid search over a set of about 20 000 range values R_j and about 8000 Doppler-values ω_k. We implement the search using the FFT-based fast match function method developed for EISCAT space debris work [5]. For large SNR, this gives the range estimate with one sample accuracy, that is, with the range resolution corresponding to the sampling interval. We get also an initial Doppler estimate with the fairly coarse FFT resolution.

The second step in the single-pulse processing is to refine the initial estimates. With the phase code used in the satellite experiment, the function $\boldsymbol{\Xi}(R, \omega)$ depends relatively slowly on R so that when determining the velocity with high accuracy, the precise value of the R does

not matter much. This allows us to separate the high-resolution determination of R from the high-resolution determination of ω, which reduces the two-parameter estimation problem to two single-parameter problems. The analysis first handles the range rate.

4.2. High resolution determination of range rate

When the range is known with one-sample resolution from the grid search, the M samples representing the received echo of the form Eq. (1) are selected from the much longer total data vector. The position of the transmitted pulse in the total data vector is known a priori. The samples of the transmitted pulse, normalised to unit amplitude, give the sampled envelope $\epsilon(t_m)$. This envelope is complex conjugated and multiplied point by point with the echo vector. With the complex conjugation, the point-wise multiplication helps to cancel, in addition to the phase code sign alternations, also a small linear phase distortion that is often present in the transmitted and hence in the received pulse as well. The result is an M-point complex-valued echo vector $\mathbf{z}'$ with elements modelled as

$$z'_m = A \exp(i\omega t_m) + \gamma_m \,. \tag{16}$$

Multiplication by a phase factor does not change the noise statistics so no prime mark is needed in γ_m. This model no more contains phase flips and therefore $\|\xi(\omega)\|^2$ is always exactly equal to M, the number of samples used.

The marginalised Bayesian solution for the frequency in Eq. (16) can be copied down from Eq. (9) and (13), essentially by replacing $\boldsymbol{\Xi}$ with $\boldsymbol{\xi}$. This gives

$$\widehat{\omega} = \arg\max_{\omega} \frac{|\mathbf{z}' \cdot \boldsymbol{\xi}(\omega)|^2}{M} \tag{17}$$

and

$$p(\omega|\mathbf{z}') = C_{z'} \exp\left\{ \frac{|\mathbf{z}' \cdot \boldsymbol{\xi}(\omega)|^2}{M\sigma^2} \right\} \,. \tag{18}$$

In addition, the complex amplitude A can be computed as

$$\widehat{A} = \frac{\mathbf{z}' \cdot \boldsymbol{\xi}(\widehat{\omega})}{M} \,. \tag{19}$$

Within the model of Eq. (16), there are no approximations involved, for $\|\boldsymbol{\xi}(\omega)\|^2$ is always exactly M, the number of samples used.

The Bayesian solution for determining the frequency of a single-frequency real-valued signal in noise was published by Jaynes and Bretthorst in the 1980s [1]. For a complex quadrature signal, solution corresponding to Eq. (17) and Eq. (18) was given by Bretthorst in 2001 [2].

The quantity to be maximised in Eq. (17) is the squared modulus of the discrete-in-time, continuous-in-frequency Fourier transform, and is called the Schuster periodogram. Equation (17) says that the frequency is found

by locating the maximum of the periodogram. Equation (18) shows that the periodogram as function of ω fully characterises the solution. In [7], we have presented a very fast approximate procedure for solving the frequency.

We now use the distribution in Eq. (18) to derive the posterior variance, which we will use as the error estimate of the single-pulse frequency. We show that the posterior density in Eq. (18) is well approximated by a Gaussian distribution in the case of high SNR, which is the case in satellite work.

The particular value of $\mathbf{z}'$ determines the location of the distribution on the frequency axis, but the overall shape of the distribution should not change much when $\mathbf{z}'$ varies a little. For high SNR, we approximate the shape as if there were no noise at all, that is, we take the measurement to be $\mathbf{z}' = A_0\boldsymbol{\xi}(\omega_0)$, and inspect the distribution as function of ω in the neighbourhood of $\widehat{\omega} = \omega_0$. We assume uniformly spaced sampling times $t_m = m\tau$ (while noting that the basic result in Eq. (17) and Eq. (18) in no way depends on uniform sampling), and get

$$\begin{aligned} |\mathbf{z}' \cdot \boldsymbol{\xi}|^2 &= |A_0|^2 \left| \sum_{m=0}^{M-1} \exp\{i(\widehat{\omega} - \omega)t_m\} \right|^2 \\ &= |A_0|^2 \left| \frac{\sin[(\widehat{\omega} - \omega)\tau M/2]}{\sin[(\widehat{\omega} - \omega)\tau/2]} \right|^2 \\ &\approx |A_0|^2 \left[M^2 - (M^4/3)(\tau/2)^2(\omega - \widehat{\omega})^2 \right]. \end{aligned} \tag{20}$$

Inserting Eq. (20) into Eq. (18) and switching from angular to linear frequency, gives

$$p(f|\mathbf{z}') \approx C_{z'} \exp\left[-\frac{(f - \widehat{f})^2}{2\sigma_f^2} \right] \,, \tag{21}$$

where the variance parameter is

$$\sigma_f^2 = \frac{3}{2\pi^2} \frac{1}{M \, \mathrm{SNR}} \frac{1}{L^2} \,. \tag{22}$$

Here $L = M\tau$ is the pulse length and $\mathrm{SNR} = |A_0|^2/\sigma^2$ is the signal to noise ratio. This result is used as the single-pulse error estimate for the Doppler frequency.

4.3. High resolution determination of range

Once the pulse position is found with one sample resolution, and the high resolution Doppler shift $\widehat{\omega}$ and the signal amplitude $\widehat{A}$ have been accurately determined, they can be taken into account in Eq. (1), leaving only a real-valued estimation problem of type

$$x_m = \epsilon(t_m - \Delta) + \eta_m \,, \ m = 0, \ldots, M - 1 \,, \tag{23}$$

where the real-valued noise η has standard deviation given by

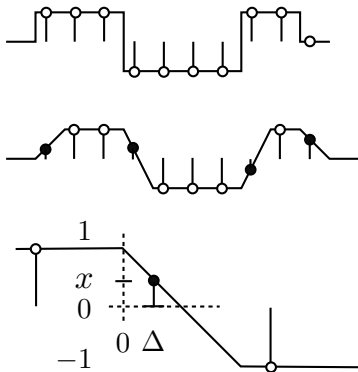$$\sigma_\eta^2 = 1/(2\,\mathrm{SNR}) \tag{24}$$

Figure 2. Determining pulse position with sub-sample resolution. The top panel shows sampling of an ideal, very-wide-band phase-coded signal. The position of that kind of signal can only be determined with the resolution of the sampling interval. The middle panel shows a more realistic situation, where the ideal signal is smoothed (averaged) by the receiver, in a way determined by the receiver's known impulse response. With duration of the impulse response equal to the sampling interval, there will be one slope sample (black dots) per phase flip. The bottom panel illustrates how the value x of a slope sample contains information about the shift Δ of the pulse with respect to the sampling times.

in terms of the SNR of the original complex signal.

The time shift Δ represents the time interval from the start of a phase flip to the next sample, as illustrated in the bottom panel of Fig. 2. The figure indicates that the information on the pulse timing is present in the pulse "slopes". The slopes are formed when filtering in the receiver smooths the initially sharp phase flips produced by the transmitter. With filtering matched to sampling rate, one gets about one sample per phase flip. In the set of phase codes used in the satellite measurement, the number of phase flips N in a pulse varies between 10 and 21. For determination of the range at a high resolution, we made use only of the slope samples and neglected the pulse front and rear ends.

Equation (23) defines a single-parameter estimation problem. In particular, there is no adjustable amplitude factor in the model function. The implication is that a match function approach analogous to Eq. (17) does not quite work now. In analogy with Eq. (17), one might be tempted to try an estimate

$$\widehat{\Delta} = \arg \max_{\Delta} \frac{|\mathbf{x} \cdot \boldsymbol{\epsilon}(\Delta)|^2}{\|\boldsymbol{\epsilon}(\Delta)\|^2}, \qquad (25)$$

where a notation $\boldsymbol{\epsilon}(\Delta) = [\epsilon(t_0 - \Delta), \ldots, \epsilon(t_{M-1} - \Delta)]^{\mathrm{T}}$ is applied. Here the numerator is just the conventional cross-correlation function often used in pattern matching. Indeed, the estimation recipe Eq. (25) possesses the required property that, without noise, the estimate recovers the actual value of the parameter (provided that in addition to the slope samples, at least one non-slope sample

is included in $\mathbf{x}$ and $\boldsymbol{\epsilon}$). Note also that the norm in the denominator depends, possibly strongly, on Δ.

In order to apply Eq. (25) for achieving sub-sample resolution in range, one should compute the shifted envelope $\boldsymbol{\epsilon}(\Delta)$ with the corresponding time resolution. One could try to design the radar measurement so that the transmission is sampled tightly enough so that an FFT-based interpolation scheme would allow recovering the continuous ϵ from its samples accurately enough. This would be the ideal way, since it requires no extra information outside the data itself. In the experiment, however, the transmission was sampled at the same rate as the reception, and our attempts in this direction have been disappointing. Therefore, in our present analysis, we have resorted to stronger modelling of the phase flip slopes in ϵ. Such an approach brings its own perils in the form of modelling errors.

We have not really inspected how good or bad the estimate Eq. (25) would be in practice. Anyway, it would only be an approximation of the exact solution given by Eq. (9). Instead, our present choice is to minimise the least squares norm, i.e. to find

$$\widehat{\Delta} = \arg \min_{\Delta} \|\mathbf{x} - \boldsymbol{\epsilon}(\Delta)\|^2, \qquad (26)$$

which is the proper Bayesian solution of Eq. (23). We derive an error estimate for this estimate later in this section.

In order to obtain a continuous-time envelope ϵ, we use the precisely known numerical impulse response of the digital back-end of the EISCAT receiver, only adding a small correction to approximately account for the impulse response of the wider bandwidth of the EISCAT analogue receiver. We further assume that the transmitted pulse itself has a bandwidth that is much larger than the bandwidth of the combined receiver, so that the phase code in the receiver front end is just equal to the ideal phase code (such as shown schematically in the top-panel of Fig. 2). With these assumptions, ϵ can be computed for all instants of time, resulting in a smoothed shape such as that illustrated in the middle panel of Fig. 2.

It would be convenient, if the slopes at the phase flips were linear like those in Fig. 2. Then Eq. (23) would pose a linear estimation problem, and the solution would be straightforward. Linear slopes are produced when the impulse response has a boxcar shape. The actual impulse response in the satellite measurement was closer to triangular in shape and its length was about 1.4 μs. As a result, the phase flip curves are not linear, and the estimation problem is also non-linear. With the 1 μs sampling interval, there will be either one or two samples per phase flip. In the case of two samples at a flip, we only used a single sample for simplicity.

It became evident in the data analysis that the model phase flip curve was inaccurate at large departures from the zero level, i.e. when the value of the sample at the flip slope was close to -1 or $+1$. This was at least partly due

to a non-ideal shape of the transmission envelope. For our final analysis results, we ended up using only slope samples with magnitudes $|x_n| < 0.7$. Although this restriction led to the rejection of large number of pulses from individual beam passes, it reduced the fit residues drastically.

The most straightforward way to estimate the sub-sample shifts of transmitted and received pulses, would be to calculate them directly from Eq. (26). Then the pulse propagation time from transmission via the target to reception, which gives the range estimate, would just be the difference of the fine-resolution times of the transmission and reception pulses. However, the length of the received pulse changes due to the Doppler shift, and this should be taken into account in the analysis at the resolutions we are aiming at. Therefore our analysis actually proceeds differently.

When an accurate range rate is already known, one could in principle account for the change of pulse length by re-interpreting the sampling times. However, we sidestep the issue by examining each phase flip individually, and calculate the time from its transmission to reception at a high accuracy. After this has been done for all the flips of the pulse, we make a properly weighted linear fit to the range estimates to get a final single-pulse range estimate for that transmission-reception cycle, and an error estimate for it.

A benefit in examining a single flip at a time is that, with a single data point only, Eq. (26) becomes trivial to solve. Denoting by $f_n(t)$ the monotonous (increasing or decreasing) slope function associated with the slope sample x_n, and by Δ_n the shift from the start of the slope to the sampling time t_n, the MAP estimate is

$$\widehat{\Delta}_n = f_n^{-1}(x_n). \qquad (27)$$

We apply this only for slope points with $|x_n| < 0.7$. An additional simplification is that, in the satellite experiment, the phase flips are programmed to be exact integer number of samples apart, so only two different functions $f_n(t)$ actually need to be tabulated, one for the "up" phase flips and the other for the "down" phase flips.

Is there some price in terms of accuracy in the single flip at a time approach compared using all flips at once? For high SNR, the answer seems to be no. We get essentially the same error estimate in both cases, at least when SNR is so high that the theory in Eq. (23) becomes essentially linear. We have not inspected the case of low SNR, which would be relevant e.g. for most space debris targets. But then the achievable range accuracy will anyway become lower, and one might not need to worry about the effect of the Doppler shift to the pulse length. Then one probably should use all flips at the same time in finding the range estimate for a single pulse.

In both cases, when assessing the error in the single-pulse range, we only account for the error in the position of the received pulse. The transmitted pulse has such a high

SNR (10^4) that the statistical error in its position is insignificant.

Consider first the position error of a single flip. Linearising the model of Eq. (23) around a delay Δ_0, so that $\Delta = \Delta_0 + \delta$, gives

$$x_n \approx f_n(\Delta_0) + \dot{f}_n(\Delta_0)\,\delta + \eta_n. \qquad (28)$$

Standard linear theory (or in this case, simply considering differentials dx_n and $d\delta$) gives for the variance σ_n^2 of the shift Δ_n of the n'th flip

$$\sigma_n^2 = \frac{\sigma_\eta^2}{[\dot{f}_n(\Delta_0)]^2} = \frac{1}{2\,\text{SNR}\,[2\,p_n(\Delta_0)]^2}\,, \qquad (29)$$

where we used Eq. (24) and also replaced the slope function's derivative by the impulse response p. The final per pulse position error is, essentially, the error of the fitted Δ in a linear fit

$$\Delta_n = kt_n + b \qquad (30)$$

where the values t_n are the times of the slope samples.

To get a rough estimate of the error for the purpose of a qualitative comparison, assume $k = 0$ in Eq. (30) so that the fitted Δ is just the weighted average of the Δ_n, where the inverses of the variances σ_n^2 are the weights. The variance of such a mean is

$$\sigma_\Delta^2 = \frac{1}{\sum(1/\sigma_n^2)} = \frac{1}{N \cdot 2\,\text{SNR}\,<2\,p(\Delta)^2>} \qquad (31)$$

where $< p(\Delta)^2 > = \sum[p_n(\Delta)]^2/N$.

Then consider the case of using all the N flips simultaneously in Eq. (26). Instead of the scalar equation Eq. (28), we have a vector-valued, single parameter, linear model where Eq. (28) provides the components,

$$\mathbf{x} - \mathbf{f_0} \approx \dot{\mathbf{f}}\,\delta + \boldsymbol{\eta}. \qquad (32)$$

The variance of the shift δ is the (single-element) covariance matrix of the linear theory of Eq. (32),

$$\sigma_\delta^2 = \left(\dot{\mathbf{f}}^{\text{T}}\frac{1}{\sigma_\eta^2}\dot{\mathbf{f}}\right)^{-1}. \qquad (33)$$

Eq. (33) reproduces Eq. (31), which shows that for the case of high SNR, our single flip at a time approach does not unnecessary lose accuracy.

5. WHAT ACCURACY TO EXPECT

The EISCAT Tromsø 930 MHz-radar operates at a power of 1.5 MW. A complex signal from a one square metre target at a range of 1000 km, as received by this radar, can reach SNR values up to about 300. In the satellite experiment, 1.92 ms phase coded pulses with interpulse period of 20 ms were transmitted and sampled continuously at the rate of one megasamples per second. The

32 m antenna's half-power beam width is about 0.6°. At the radar zenith, it takes 1.5 s, i.e. 75 interpulse periods, for a polar orbiting satellite at 1000 km altitude to cross that angle.

One expects from Eq. (22) that, at the beam centre, the 1-sigma error of a single pulse Doppler frequency is about 0.25 Hz. Then the velocity error is about $4\,\mathrm{cm\,s}^{-1}$. To get a rough estimate for the expected range error from Eq. (29) and Eq. (31), assume a constant receiver impulse response of $1.0\,\mu s$ duration, so that the constant phase flip slope is $\dot{f} = 2\,(\mu s)^{-1}$. Then the single phase flip position error σ_n in Eq. (29) is $1/(2\sqrt{2\times 300})\,\mu s = 0.02\,\mu s$, which corresponds to a range error of 3 m. Assuming ten such flips for the per-pulse range estimate, the error is expected to drop by about $\sqrt{10}$ to about 1 m.

It is less straightforward to estimate the error after the per-pulse estimates are utilised in Eq. (14) and Eq. (15) to produce the final range and Doppler velocity estimates for a single beam pass. We may still expect the errors scale roughly proportional to the inverse of the square root of the number of points used in the fits, by a factor of 5–10 (depending how large fraction of the pulses can actually be used). This brings the final velocity error to a few millimetres per second and the final range error to a few tens of centimetres.

The SNR at the beam center in the 154 beam pass events measured on 1-Dec-2010 varied between 1 dB (Jason at 2400 km range) and 45 dB (Metop at 840 km range). Fourteen events had SNR compatible with the above estimate, with a peak SNR between 200 and 400. For those 14 events, the 1-sigma range error varied between 7 cm and 19 cm, while the 1-sigma error in range rate varied between 0.4 cm/s and 1 cm/s.

In Fig. 3 we show the range and range rate error for all 154 events. The figure is broadly compatible with the above estimate. The figure shows three things. First, it suggests that our analysis machinery probably implements our basic theoretical error estimates Eq. (22) and Eq. (29) and the error propagation correctly, or at least consistently. Second, it shows as a function of SNR, what kind of accuracy one can expect from a fairly standard EISCAT measurement if all the systematic errors can be ironed out. Third, already somewhere near $\mathrm{SNR} = 5\,\mathrm{dB}$, the error model starts to break down, especially with the range data. This probably indicates that the whole single-pulse based analysis is becoming problematic. This in turn suggests that, without coherent integration of some kind, our improved analysis cannot be applied to typical space debris targets.

6. SYSTEMATIC ERRORS

In our analysis, there are several potential sources of systematic error that need to be kept in mind when using the analysis results for orbit determination purposes. A trivial (but embarrassing) problem is that the geographic
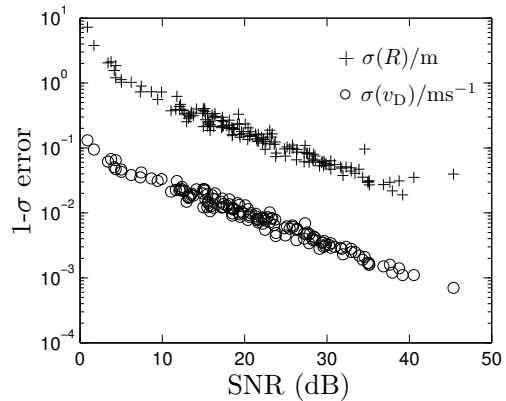

Figure 3. One-sigma statistical range errors (+) and range rate errors (○) in the 154 beam pass events measured at EISCAT on 1-Dec-2010.

position (latitude, longitude, altitude) of the Tromsø radar antenna is currently under dispute. The coordinates, and especially the longitude, that one gets from modern maps, including those given by Google Earth, handheld GPS receivers, as well as the local area maps provided by the Norwegian land survey, differ by several tens of meters from the coordinates given by EISCAT official web site.

A second, a somewhat trickier, problem is defining and determining a point, presumably somewhere within the antenna structure, to which the pulse propagation time measurements should be referred to; that is, what precise point the "antenna position" refers to. There is no fixed centre of rotation of the Tromsø antenna. Peculiarities of the antenna construct have the consequence that when the antenna pointing in azimuth or elevation is changed, the length of the ray path from the antenna to the target changes by a few meters even if the true satellite distance would be the same. This means that the antenna position to be used in orbit calculation depends on the pointing direction by several metres.

A third issue is related to signal delays in the receiver. The directly estimated pulse transmit and receive times refer to the position of the pulse's leading edge with respect to the sampling instances (the UTC time of each sample is known within a fraction of a microsecond, and the time is stable within a few nanoseconds between transmission and reception from pulse to pulse). Before getting sampled, both the echo signal and the transmission sample signal have travelled a lengthy, but unknown, distance in the receiver. This travel path is almost, but not quite, the same for both signals. The result is that, when the pulse propagation time is estimated as the difference of the two signals' measured leading edge times, the receiver delays almost, but not precisely, cancel out. This may cause a constant error of maybe a few metres in the range estimates.

A fourth issue, related to the antenna geometry, is the extra delays of the signal due to the antenna's Cassegrain

optics. Finally, there is also the issue of delays in the ionosphere.

All these sources of errors need to be accounted for when using the analysis results for orbit determination, although they do not directly show up in the analysis results themselves. But there are effects that will show up in the range and velocity fit residues. These are related to problems in the signal model of Eq. (1).

The most obvious problem in the signal model is that the amplitude parameter A is a constant, which corresponds to assuming a point-like, structureless, target. But even the smallest of the campaign targets, the Proba-1 satellite which, according to its web page is a cube of the size $60 \times 60 \times 80$ cm, is more than two radar wave-lengths in size, and so the reflected pulse can be subject to strong interference effects which can modulate both the echo phase and the amplitude. All the other targets are several metres or even tens of meters in size, and are quite irregular in shape with possibly multiple strong scattering centres, which makes the point-target assumption even more incorrect.

The manifestly non-zero size of a target means that, even if the target were stabilised in an inertial frame, it would appear be rotating in the radar frame. This would show up in the Doppler velocity. The modulation of the signal amplitude due to interference can disturb the phase flip shapes that our range estimates depend on. And even if the target were very smooth, just its finite size would already mean that it takes time for the target to become fully illuminated, and this would also affect the signal shape. For instance, it could make the observed phase flip slopes longer and less steep.

A second problem in the signal model is that we assume a specific form of the receiver impulse response on one hand, and a very wide band, sharp phase flip in transmission on the other hand, when we compute the code envelopes ϵ, and both of these assumptions can be wrong. They do not need to be much wrong to become visible in the fit residues.

When fitting results from individual pulses to the beam pass model of Eq. (14), it becomes clear that the scatter in the ranges and range rates is considerably larger than their statistical errors suggest. Quite often, the residue does not look like noise, but there are slow semi-periodic variations of the same general size or slightly larger than the 1-sigma error bars in data from the individual pulses.

7. CONCLUSION

Based mainly on the behaviour of the fit residues, it seems probable that the actual uncertainty in the per beam passage ranges and range rates can be up to an order of magnitude larger than the statistical error bars suggest. That is, the accuracy may not be much better than what one could get already from the single-pulse analysis, typically

a few metres in range, and several centimetres per seconds in range rate. But even this is a significant improvement over EISCAT's original analysis of the 2010 data. It would be interesting to see the updated results tested for orbit determination purposes.

REFERENCES

1. Bretthorst G., (1987). Bayesian Spectrum Analysis and Parameter Estimation, Ph.D thesis, Washington University, St. Louis, MO

2. Bretthorst G., (2001). Generalizing the Lomb-Scargle peridiogram, *Bayesian Inference and Maximum Entropy Methods in Science and Engineering*, Paris, Ali Mohammad-Djafari (ed.). American Institute of Physics Proceedings, **569**, 241-245

3. Fontdecaba i Baig J., Martinerie, F., Sutter,.M, Martinot, .V, Fletcher, E., (2011). Radar tracking campaigns for ESA CO-VI, Proceedings of European Space Surveillance Conference, Madrid, 7-9 June

4. Markkanen, J., Lehtinen, M., Huuskonen, A., Väänänen, A., (2002). Measurements of small-size debris with backscatter of radio waves, Final report, ESOC Contract No. 13945/99/D/CD

5. Markkanen J., Lehtinen, M., Landgraf, M., (2005). Real-time space debris monitoring with EISCAT, *Advances in Space Research*, **35**, 1197-1209

6. Markkanen, J., Nygrén, T., Markkanen, M., Voiculescu, and Aikio, A., (2013). High-precision measurement of satellite range and velocity using the EISCAT radar, *Submitted in Ann. Geophys.*

7. Nygrén, T., Markkanen, J., Aikio, A., and Voiculescu, M., (2012). High-precision measurements of satellite velocity using the EISCAT radar, *Ann. Geophys.*, **30**, 1555-1565